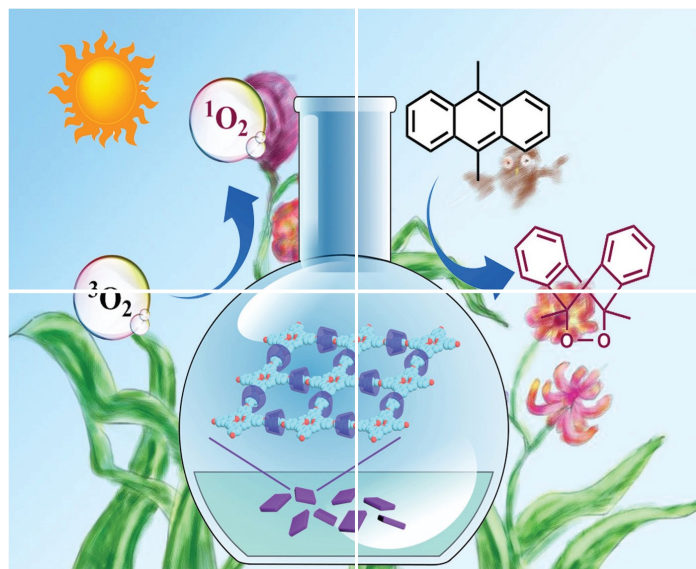


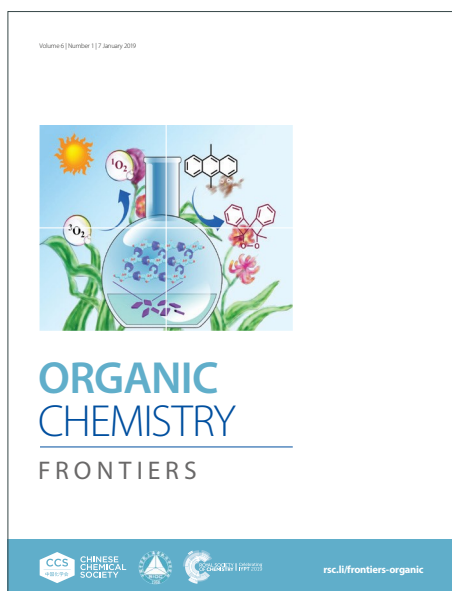
ORGANIC CHEMISTRY

FRONTIERS

Accepted Manuscript



This article can be cited before page numbers have been issued, to do this please use: L. Menduti, C. C. Baldoli, M. Bolte, S. Manetto, C. Villani, M. Penconi, S. Grecchi, S. ARNABOLDI, G. Mazzeo, G. Longhi, A. Virovets, H. Lerner, M. Wagner and E. Licandro, *Org. Chem. Front.*, 2025, DOI: 10.1039/D4QO01897D.



This is an Accepted Manuscript, which has been through the Royal Society of Chemistry peer review process and has been accepted for publication.

Accepted Manuscripts are published online shortly after acceptance, before technical editing, formatting and proof reading. Using this free service, authors can make their results available to the community, in citable form, before we publish the edited article. We will replace this Accepted Manuscript with the edited and formatted Advance Article as soon as it is available.

You can find more information about Accepted Manuscripts in the [Information for Authors](#).

Please note that technical editing may introduce minor changes to the text and/or graphics, which may alter content. The journal's standard [Terms & Conditions](#) and the [Ethical guidelines](#) still apply. In no event shall the Royal Society of Chemistry be held responsible for any errors or omissions in this Accepted Manuscript or any consequences arising from the use of any information it contains.

(BO)₂-doped tetrathia[7]helicenes: synthesis and properties change induced by “BO bonds inversion”

Received 00th January 20xx,
Accepted 00th January 20xx

DOI: 10.1039/x0xx00000x

Luigi Menduti,^{*a,b} Clara Baldoli,^c Simone Manetto,^d Claudio Villani,^d Marta Penconi,^e Sara Grecchi,^a Serena Arnaboldi,^a Giuseppe Mazzeo,^f Giovanna Longhi,^f Michael Bolte,^b Alexander Virovets,^b Hans-Wolfram Lerner,^b Matthias Wagner^{*b} and Emanuela Licandro^a

Helical distortion of polyaromatic hydrocarbons gives rise to a special class of π -conjugated systems, namely helicenes. Owing to their configurational stability and easily tunable optoelectronic properties (*via* heteroatom-doping), helicenes have recently come to the fore as building blocks for applications in material science (CP-OLEDs, chiroptical switches); in this context, boron-doped helicenes are particularly promising. Herein, we report the synthesis of the new (BO)₂-doped tetrathia[7]helicene **2**, derived by the formal inversion of (Mes)B–O moieties in the (previously reported) isomer **1**. Theoretical characterization of **2**, and comparison with **1**, revealed that the inversion of the BO vectors promotes the extension of the LUMO *via* the central thiophene-benzene-thiophene fragment (and not *via* the terminal thiophene rings, as in **1**), resulting in a considerable lowering of the LUMO energy ($E_{\text{LUMO}}(\mathbf{2}) = -2.22$ eV vs. $E_{\text{LUMO}}(\mathbf{1}) = -1.65$ eV). Spectroscopic studies revealed that the “BO bonds inversion” also contributes to the narrowing of the energy gap ($E_g^{\text{opt}}(\mathbf{2}) = 2.90$ eV vs. $E_g^{\text{opt}}(\mathbf{1}) = 3.16$ eV) and causes a significant red-shift of the absorption/emission bands (≈ 40 nm). Interestingly, besides low fluorescence quantum yield ($\Phi_{\text{PL}}(\mathbf{2}) = 7\%$), **2** shows detectable Circularly Polarized Luminescence ($g_{\text{lum}} = 0.8 \times 10^{-3}$) and pronounced phosphorescence at low temperature (77 K). (*P*)-/(*M*)- enantiomers of **2** were successfully separated by CSP-UHPLC and proved to be stable ($\Delta G_{\text{enant}}^\ddagger = 29.4 \pm 0.1$ kcal/mol at 353 K). Racemization studies combined with theoretical calculations, confirmed that BO-doping is an extremely perturbative tool for tuning the mechanical rigidity of tetrathia[7]helicenes ($\Delta G_{\text{enant}}^\ddagger(\mathbf{2})$ is 10 kcal/mol lower than $\Delta G_{\text{enant}}^\ddagger(\mathbf{7TH})$).

Introduction

Helicenes, which are non-planar, screw-shaped chiral structures composed of ortho-fused aromatic or heteroaromatic rings, represent a unique class of polycyclic aromatic hydrocarbons (PAHs).¹ Configurationally stable helicenes show peculiar chiroptical and optoelectronic features suitable for their application in the field of materials science.^{2,3}

Recently, the so-called heteroatom doping, based on the replacement of selected carbon atoms by other p-block elements,⁴ opened new perspectives in helicene chemistry allowing the modulation of their electronic structures and optoelectronic properties. The most commonly used doping elements to date are Si, N, P, O and S, but recently several examples of B-atom introduction have been described.⁵ Only a limited number of purely B(sp²)-doped helicenes and chiral PAHs incorporating helicene subunits have been reported so far,⁶ while in most of the examples, C=C double bonds are replaced by B(sp²)-N/B(sp²)-O^{7,8} or B(sp³)-N bonds.⁹ Our groups have recently contributed to this field by establishing the synthesis and investigating the optoelectronic and chiroptical properties of the first doubly BO-doped tetrathia[7]helicene **1**¹⁰ (Figure 1).

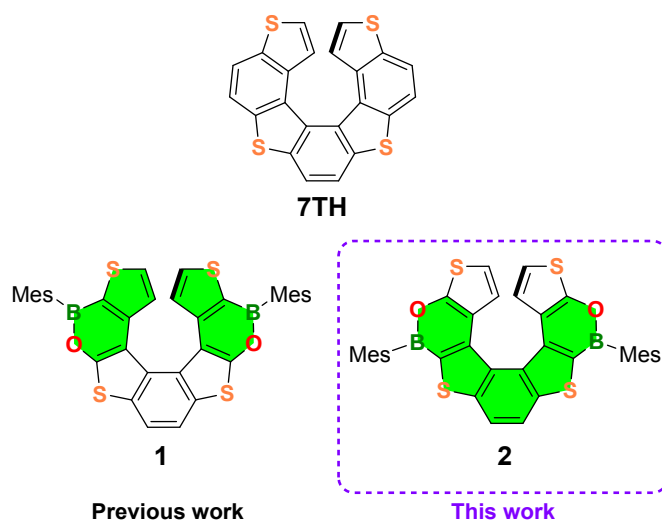


Figure 1. Structures of the parent tetrathia[7]helicene (**7TH**), the previously reported **1** and the newly developed (BO)₂-helicene **2**. Mes = 2,4,6-trimethylphenyl (mesityl). The LUMO extension in the structures **1** and **2** is highlighted in green.

Although **1** showed poor optical performance ($\Phi_{\text{PL}} = 6\%$, $E_g^{\text{opt}} = 3.16$ eV), our studies have demonstrated that the incorporation of two BO fragments into the tetrathia[7]helicene (**7TH**; Figure 1) scaffold provides a powerful tool to manipulate the mechanical rigidity, the chiroptical properties, and the electron distribution across the helix.

With the aim of thoroughly investigating the effect of BO doping of the **7TH** framework to obtain helicenes with improved photophysical features, we designed the new (BO)₂-helicene **2**, an isomer of **1**, derived by the formal inversion of the BO bonds in the two oxaborine rings (Figure 1).

^a Dipartimento di Chimica, Università degli Studi di Milano. Via C. Golgi 19, 20133, Milano (Italy).

^b Institut für Anorganische Chemie, Goethe-Universität Frankfurt. Max-von-Laue-Strasse 7, 60438, Frankfurt am Main (Germany).

^c CNR Istituto di Scienze e Tecnologie Chimiche Giulio Natta. Via C. Golgi 19, 20133, Milano (Italy).

^d Dipartimento di Chimica e Tecnologie del Farmaco, Sapienza Università di Roma. P.le A. Moro 5, 00185, Roma (Italy).

^e CNR Istituto di Scienze e Tecnologie Chimiche Giulio Natta, Via G. Fantoli 16/15, 20133 Milano (Italy) and SmartMatLab Center, via C. Golgi 19, 20133 Milano (Italy).

^f Dipartimento di Medicina Molecolare e Traslationale, Università di Brescia. Viale Europa 11, 25123, Brescia (Italy).

(BO)₂-helicene **2** was tailored based on our previous results, which showed that the LUMO of **1** (highlighted in green in Figure 1) is mainly localized on the B-substituted terminal thiophene rings,¹⁰ while the HOMO, as in **7TH**,¹¹ is spread over the entire helix (for DFT calculations see Figure 6, Figure S49).

These results suggested that the position of the B atoms could be crucial for the extension of the LUMO across the helix, with only minor effects on the HOMO distribution/energy (as in the case of boron-doped planar polyaromatics).^{4c} The inverted positions of the BO bonds in **2** were therefore expected to promote the extension of the LUMO *via* the central thiophene-benzene-thiophene fragment rather than *via* the terminal thiophene rings only (Figure 1). This could provide a helicene with extended and energetically lowered LUMO, narrowed HOMO-LUMO energy gap and, improved optoelectronic performance.

Herein we report the synthesis of the (BO)₂-helicene **2**, along with its optoelectronic and chiroptical properties and a comparison with those of the previously reported (BO)₂-helicene isomer **1**.¹⁰ Moreover, we describe attempts to synthesize the (BO)-doped helicene **3** (Scheme 2a), formally derived by the replacement of the central C=C bond in **7TH** with a (Mes)B-O fragment. Although the target BO-helicene **3** was not obtained, the investigation of two different synthetic approaches provided important information for the design of new derivatives and allowed us to isolate the penta-fused intermediate **11** (see Results and Discussion).

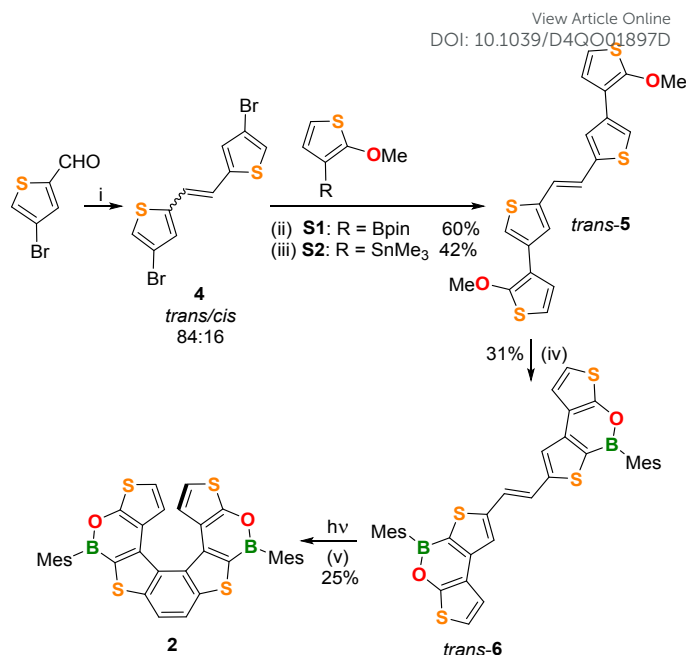
Results and Discussion

Synthesis, NMR spectra, and X-ray characterization of **2**

The (BO)₂-helicene **2** was prepared in four steps, starting from 4-bromothiophene-2-carbaldehyde¹² (Scheme 1), which was converted into the alkene **4** in 89% yield (*trans*:*cis* = 84:16) *via* a McMurry coupling. The *trans* isomer was isolated in 82% yield by washing the crude product with Et₂O.

The next step was performed on *trans*-**4** and involved Suzuki or Stille coupling with the corresponding partners 2-(2-methoxythiophen-3-yl)-1,3,2-dioxaborolane **S1** or (2-methoxythiophen-3-yl)trimethylstannane **S2** and furnished the alkene *trans*-**5** in 60% and 42% yield, respectively. Although Suzuki coupling gave a better yield, our preferred route for *trans*-**5** remains Stille coupling, due to the easier preparation and purification of the stannane **S2**. The subsequent two-fold borylation of *trans*-**5** was performed by demethylative borylation with BCl₃/[*n*Bu₄N]/Et₃N¹³ in chlorobenzene at 135 °C, followed by the addition of MesMgBr. In this way, the alkene *trans*-**6** was obtained in 31% yield after purification.

The structures and the *trans*-configurations of the double bonds in intermediates **4**, **5**, and **6** were confirmed by X-ray crystallography (Figure S36-S38). The last reaction to obtain the helicene structure was a Mallory photocyclization¹⁴ involving as first step the isomerization of *trans*-**6** to *cis*-**6**, which afterwards cyclized to give **2**. We first investigated the *trans*→*cis* isomerization. To this end, an



Scheme 1. (i) 2.6 equiv Zn, 1.2 equiv TiCl₄, THF, 0–15 °C; (ii) 2.4 equiv **S1** (R = Bpin), Pd(PPh₃)₄ 10 mol%, 4 equiv NaOH (3 M), THF, 80 °C, 15h; (iii) 2.1 equiv **S2** (R = SnMe₃), Pd(Pt-Bu₃)₂ 10 mol%, toluene, 80 °C, 17h; (iv) 2.2 equiv BCl₃, 2 equiv Et₃N, 2.4 equiv [*n*Bu₄N]Cl, chlorobenzene, 135 °C, then THF, 6 equiv MesMgBr; (v) 405 nm LED, C₆D₆, r.t., 1.5 h. Mes = 2,4,6-trimethylphenyl (mesityl).

NMR tube charged with a non-degassed C₆D₆ solution of *trans*-**6** was irradiated with a 405 nm LED lamp and the reaction progress was monitored by ¹H NMR. Surprisingly, this test showed that not only *trans*-**6** smoothly isomerizes to *cis*-**6** but also that *cis*-**6** undergoes photocyclization to give **2**, even in the absence of an added oxidant (e.g. I₂; differently from what was required for the synthesis of **1**).¹⁰ In light of these results, we then performed the synthesis of **2** under the same conditions: four NMR tubes charged with *trans*-**6** and C₆D₆ (10 mg/1mL) were simultaneously irradiated with the 405 nm LED lamp until the almost complete disappearance of the alkene precursor (1.5 h; NMR-spectroscopic control). The NMR solutions were then combined and, after chromatographic purification, (BO)₂-helicene **2** was isolated in 25% yield.

NMR characterization of the new (BO)₂-helicene **2** was done along with a comparison with the chemical shifts of the isomeric helicene **1** (Figure 2a,b). The inversion of the BO-bonds in the oxaborine rings causes a substantial upfield shift of the diagnostic ¹H and ¹³C signals of the terminal thiophene rings.

For instance, in **2**, the protons at the α and β positions of the terminal thiophene rings substituted with an electron-donating O atom (O-thiophene) resonate at 6.93 and 6.52 ppm, respectively, whereas in the corresponding isomer **1** they are significantly deshielded due to the electron-withdrawing effect of the B atom (B-thiophene) and resonate at 7.37 and 7.19 ppm (cf. parent **7TH**: 6.83, 6.67 ppm). The same trend is observed for the ¹³C shifts: **2** C(α) and C(β) resonate at 123.0 and 112.4 ppm, respectively, but are significantly deshielded in **1** (C(α) = 135.6 ppm, C(β) = 126.5 ppm).

1
2
3
4
5
6
7
8
9
10
11
12
13
14
15
16
17
18
19
20
21
22
23
24
25
26
27
28
29
30
31
32
33
34
35
36
37
38
39
40
41
42
43
44
45
46
47
48
49
50
51
52
53
54
55
56
57
58
59
60

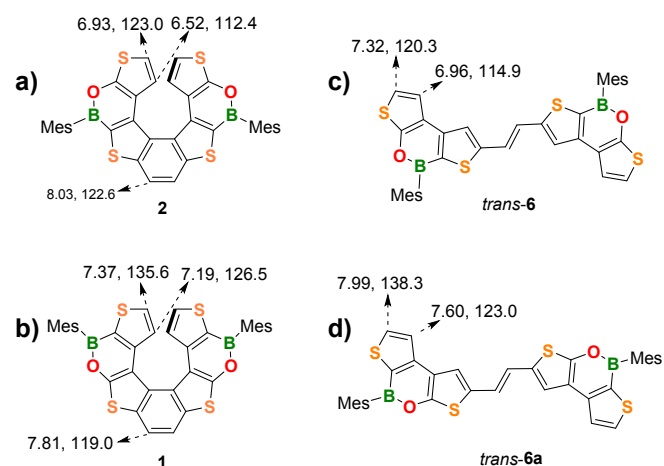


Figure 2. Comparison of diagnostic ^1H and ^{13}C NMR resonances (CDCl_3) of the two $(\text{BO})_2$ -helicenes **1** and **2** and of the corresponding *trans*-alkenes **6a** and **6**.

A similar behavior is observed for the corresponding alkene precursors *trans*-**6** and *trans*-**6a** for both the $\text{H}(\alpha)/\text{C}(\alpha)$ and $\text{H}(\beta)/\text{C}(\beta)$ resonances (Figure 2c,d). Due to the proximity of the electron-withdrawing B atoms, the protons/carbons of the central benzene ring in **2** are deshielded (8.03/122.6 ppm) with respect to those at the same positions in **1** (7.81/119.0 ppm).

Interestingly, the α and β protons of the terminal thiophene rings of **2** are more shielded than those of its planar precursor *trans*-**6** (6.93/6.52 ppm vs. 7.32/6.96 ppm). This effect can be attributed to the helical 3D-structure, in which each terminal thiophene ring falls into the shielding region of the corresponding ring in the opposite helicene wing. $(\text{BO})_2$ -helicene **1** and its precursor *trans*-**6a** show the same trend.

The crystal structure of **2** was determined by single-crystal X-ray crystallography using the high-flux DESY Petra III synchrotron source. **2** crystallizes as racemic mixture of the (*P*)- and (*M*)-enantiomers in the monoclinic crystal system (Figure 3a). **2** shows a dihedral angle between the two terminal thiophene rings of $58.36(6)^\circ$ (Figure 3b), significantly larger than that of **1** ($50.26(9)^\circ$)¹⁰ and **7TH** ($48.6(1)^\circ$),¹⁵ while the associated intramolecular centroid...centroid distances have comparable values (4.299(4) Å for **2**; 4.153(6) Å for **1**).

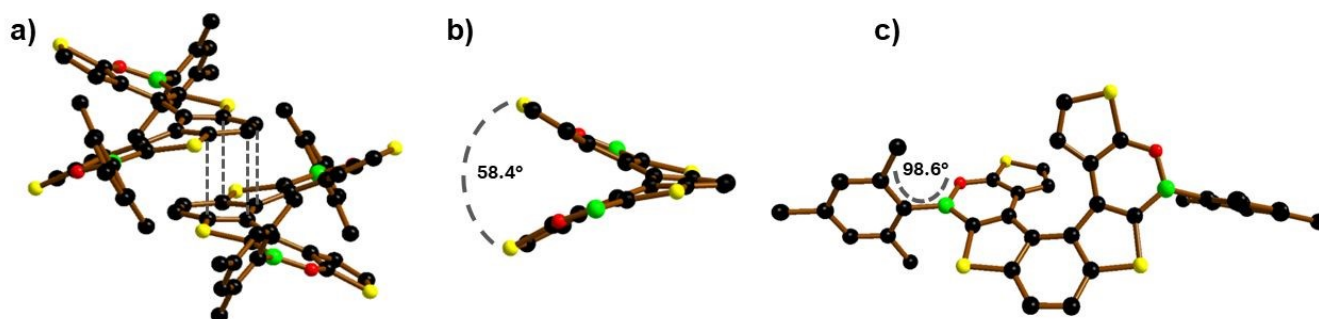


Figure 3. a) π -stacking interaction between a (*P*)/(*M*)-pair of **2** with H atoms omitted for clarity; ¹⁸ grey lines indicate the shortest intermolecular C...C contacts. b) Dihedral angle between the terminal thiophene rings of (*P*)-**2**; Mes rings are omitted for clarity. c) Front view of (*P*)-**2**. B: green, C: black, O: red, S: yellow spheres.

As for **1**, the central benzene ring of **2** is twisted (Figure 3c) as evidenced by the torsion angle of -10.5° (9.7° for **1**) between the $(\text{H})\text{CC}(\text{H})$ vector and the opposite CC bond.

Contrary to **1** and similar to most of the Mes-protected B-doped polycyclic aromatic hydrocarbons (PAHs),¹⁶ the Mes substituents of **2** are nearly orthogonal to the oxaborine rings (Figure 3c), as evidenced by the Mes//O-B-C dihedral angle ($98.6(2)^\circ$ for **2**; $59.0(5)^\circ$ and $58.6(6)^\circ$ for **1**). In both **2** and **1** the *ortho*- CH_3 groups of the Mes substituents are positioned at approximately 4 Å to the $\text{CH}(\beta)$ atoms of the opposite thiophene rings, thus excluding that the different Mes orientations in the two $(\text{BO})_2$ -helicenes could be caused by steric factors (e.g. H/H clashes). The reason for the two different orientations apparently lies in the crystal packing of **1** and **2**.

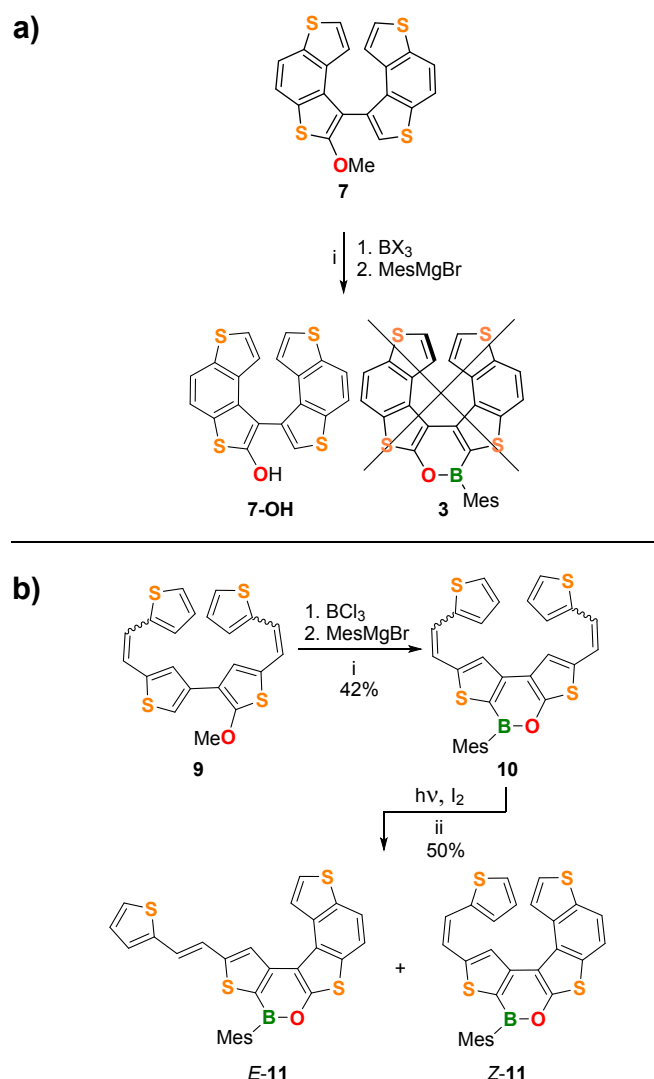
The B-O bond lengths of **2** (1.393(3) Å) are slightly shorter than those of **1** (1.402(4) and 1.401(5) Å), but longer than those of the reference compound 9-mesityl-10,9-oxaboraphenanthrene (av. B-O = 1.378 Å; av. Mes//O-B-C = $104.1(3)^\circ$ and $84.8(3)^\circ$ for two crystallographically independent molecules in the asymmetric unit).¹⁷ In the crystal, alternating molecules of (*P*)- and (*M*)-**2** form infinite rods by means of π -stacking interactions between the central benzene rings (Figure 3a; similar to **7TH**).¹⁵ The corresponding intramolecular centroid...centroid distances are 3.666(4) Å, and the shortest intermolecular C...C contacts are 3.552(4) and 3.666(4) Å (grey lines in Figure 3a). As for **1**, the shortest *intermolecular* S...S distances are smaller than the *intramolecular* ones (3.665(5) and 6.140(5) Å, respectively, for **2**; 3.9911(14) and 5.8156(2) Å, respectively, for **1**).

Synthesis attempts for **3**

Next, we attempted the synthesis of the (BO) -helicene **3** (Scheme 2a), formally derived by the replacement of the central C=C bond of **7TH** with a (Mes)B-O fragment.

To this end, we pursued two different synthetic strategies (Scheme 2a,b). The first approach involved the late-stage borylation of **7** (Scheme 2a; see the SI for details of its synthesis). In the second approach, the oxaborine ring is constructed first (*via* borylative cyclization **9**→**10**; see the SI for the synthesis of **9**), and the obtained bis-olefinated oxaborine **10** is then subjected to Mallory photocyclization (Scheme 2b).

1
2
3
4
5
6
7
8
9
10
11
12
13
14
15
16
17
18
19
20
21
22
23
24
25
26
27
28
29
30
31
32
33
34
35
36
37
38
39
40
41
42
43
44
45
46
47
48
49
50
51
52
53
54
55
56
57
58
59
60



Scheme 2. a) (i) 1.5 equiv BCl_3 or BBr_3 , 1 equiv Et_3N , 1.2 equiv $[\text{nBu}_4\text{N}]$, chlorobenzene, 135°C , then THF, 3 equiv MesMgBr ; b) (i) 1.1 equiv BCl_3 , 1 equiv Et_3N , 1.2 equiv $[\text{nBu}_4\text{N}]$, chlorobenzene, 135°C , then THF, 3 equiv MesMgBr ; (ii) 385 nm LED, 2.1 equiv I_2 , 200 equiv propylene oxide, C_6H_6 , r.t., 3.5 h.

Unfortunately, the borylative cyclization $7 \rightarrow 3$ failed for BCl_3 and BBr_3 ; only the hydroxy derivative **7-OH** was isolated besides a small amount of unidentified products (Scheme 2a; see the SI for details, Table S1). The crystal structure of the precursor compound **7** (Figure S39) indicates that the final B–C bond-forming step would have to be enforced against adverse steric factors and is therefore unfavorable. In contrast, borylation of the more flexible bis-olefin **9** (see the SI for details of its synthesis) gave the bis-olefinated oxaborine **10** in satisfactory yield (42%) as a mixture of four *E/Z* isomers after chromatographic purification. Treatment of the mixture with *n*-pentane allowed the isolation of crystals of *E,E*-**10**, the configuration of which was confirmed by single-crystal X-ray diffraction (Figure 4a, Figure S42). Photocyclization of **10** was carried out on the mixture of isomers in benzene solution by irradiation with a 385 nm LED lamp for 3.5 h at room temperature in the presence of 2 equiv. of I_2 and excess propylene oxide as HI scavenger (Scheme 2b).¹⁹ In this way, the penta-fused product *E/Z*-**11** was obtained in 50% yield as an

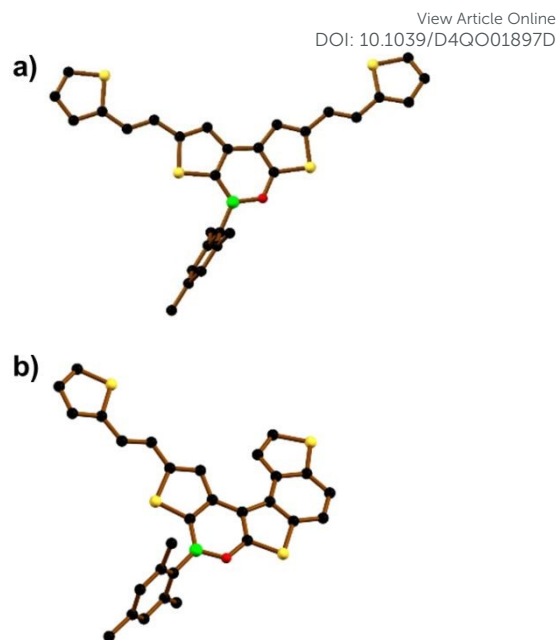


Figure 4. Solid-state structures of a) *E,E*-**10** and b) *E*-**11**. Hydrogen atoms are omitted for clarity. B: green, C: black, O: red, S: yellow spheres.

almost equimolar mixture of the *E* and *Z*-isomers. We found no indication for the formation of **3**. ^1H NMR analysis of *E/Z*-**11** allowed the assignment of most of the proton resonances of both structures (see the SI). An X-ray diffraction study of single crystals of *E*-**11** confirmed that the photocyclization had occurred at the “O-thiophene” double bond (Figure 4b, Figure S43).

Spectroscopic, Electrochemical, Theoretical, and Chiroptical Characterization of **2**

The electrochemical, spectroscopic, and chiroptical properties of the new $(\text{BO})_2$ -helicene **2** were investigated by cyclic voltammetry, UV/Vis and fluorescence spectroscopy, as well as chiral HPLC analysis, and compared with the corresponding properties of isomer **1**.

Cyclic voltammetry measurements on **2** (THF, $[\text{nBu}_4\text{N}][\text{PF}_6]$; referenced against the FcH/FcH^+ couple) showed two irreversible reduction processes with peak potentials of $E_{\text{pc}}^{\text{I}} = -1.66$ V and $E_{\text{pc}}^{\text{II}} = -2.36$ V in the cathodic scan and an irreversible oxidation peak in the anodic scan ($E_{\text{pa}} = 0.82$ V; Figures S28, S29, and Table S3). Helicene **2** is therefore easier to reduce than its isomer **1** ($E_{\text{pc}}^{\text{I}}(\mathbf{1}) = -2.83$ V). Consequently, the electrochemically determined LUMO energy of **2** ($E_{\text{LUMO}} = -3.14$ eV) is also significantly lower than that of **1** ($E_{\text{LUMO}} = -1.97$ eV), thus confirming that the B–O-bond inversion contributes markedly to the stabilization of the LUMO.

The molar absorptivity and emission spectra of **2** and **1** (*c*-hexane) are shown in Figure 5a; the data are summarized in Table 1. Both compounds show an absorption band below 300 nm and a second, more structured band at lower energy, which is red-shifted in **2** and characterized by a lower absorption coefficient relative to **1**. Consequently, the energy gap between the frontier orbitals is narrowed ($E_g^{\text{opt}}(\mathbf{2}) = 2.90$ eV vs. $E_g^{\text{opt}}(\mathbf{1}) = 3.16$ eV). The emission

spectrum of **2** shows a band with well-resolved vibrational fine structure and a maximum at 446 nm which similar to the absorption band, is bathochromically shifted with respect to the spectrum of **1**. The photoluminescence quantum efficiency of **2** remains unchanged, $\Phi_{\text{PL}} = 7\%$ (*c*-hexane; cf. **1**: $\lambda_{\text{em}} = 411$ nm, $\Phi_{\text{PL}} = 6\%$; **7TH**: $\lambda_{\text{em}} \approx 405$ nm, $\Phi_{\text{PL}} = 6\%$)²⁰ and the lifetime of the excited state is $\tau = 0.82$ ns.

To gain insight into the origin of the low quantum efficiency of **2**, low-temperature photoluminescence spectra (77 K) were measured. To avoid degradation of **2** in 2-MeTHF (which usually contains peroxides), measurements were carried out in a frozen toluene matrix; for comparison, corresponding spectra of the helicene precursor *trans*-**6** and the mesityl dithienooxaborine (**MesDFOB**) subunit have also been included in Figure 5b.

At 77 K, the fluorescence emission of **2** between 400 and 530 nm overlaps with the room temperature photoluminescence in *c*-hexane and the corresponding average lifetime of the singlet excited state is $\tau = 1.09$ ns. Interestingly, at low temperature, we observed a long-wavelength photoluminescence, between 530 and 800 nm, not present at room temperature. This emission corresponds to phosphorescence from the triplet excited state with a typical lifetime of $\tau = 63.3$ ms. Both fluorescence and phosphorescence signals are highly structured and with spacing of about 1300 and 300-700 cm^{-1} , respectively, as observed for similar thia-helicene and carbohelicene structures reported in the literature.^{11,21} In particular, the low-frequency vibronic progression of the phosphorescence band is associated with breathing vibrational modes, so-called "helix breathing".^{11,22} The observed phosphorescence of **2** results from the population of the triplet state by intersystem crossing from the singlet excited state and the subsequent relaxation of the triplet state by radiative processes. In this type of structure, these spin-forbidden singlet-triplet transitions become partially allowed by the enhanced spin-orbit coupling arising from two different contributions: the helically twisted molecular scaffold and the presence of heavy sulfur heteroatoms along the conjugated system. Notably, phosphorescence emission was observed also in our previous studies on α -dimesitylboryl benzodithiophene systems²³ (resembling the B-thiophene-benzene-thiophene-B fragment of **2**) and in tetrathia[7]helicene derivatives.¹¹

Under the same conditions, no phosphorescence was detected for the more flexible precursor *trans*-**6**, likely due to rotational

deactivation processes. Interestingly, intense phosphorescence was also observed at 77 K for the dithienooxaborine model compound **MesDFOB**, albeit at much shorter wavelengths than in the case of **2** (Figure 5b). Overall, the photophysical characterization of **2** showed that the introduction of two BO moieties into the parent **7TH** results in a red-shift of the phosphorescence emission and an enhanced phosphorescence/fluorescence ratio (for low-temperature emission measurements on **7TH** in 2-MeTHF see reference¹¹).

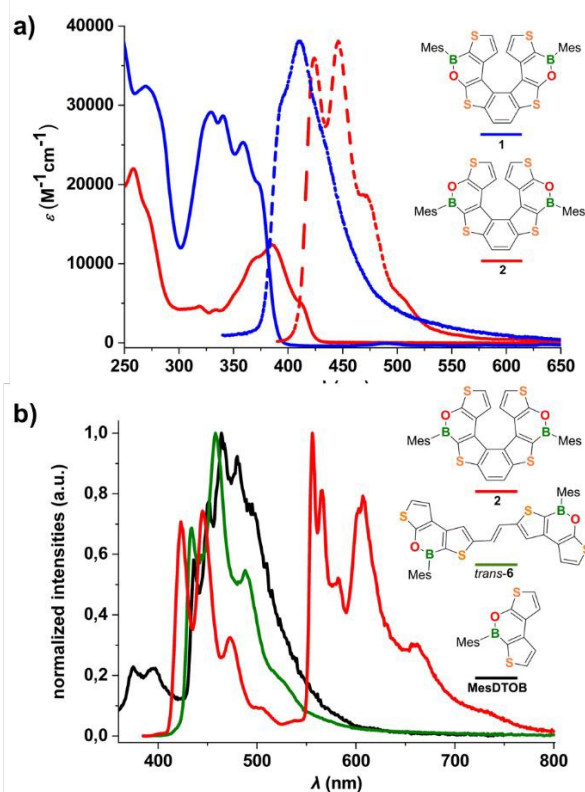


Figure 5. a) Molar absorptivity (solid lines) and emission (dashed lines) spectra of **2** (red) and **1** (blue) in *c*-hexane. b) Low-temperature emission spectra of **2** (red), *trans*-**6** (green) and **MesDFOB** (black) in a frozen toluene matrix (77 K).

Table 1. Photophysical data of **2**, *trans*-**6** and **MesDFOB** in *c*-hexane at room temperature and in toluene at 77K.

	<i>c</i> -hexane, r.t. ^[a]				toluene, 77 K						
	λ_{abs} [nm] (ϵ [$\text{M}^{-1} \text{cm}^{-1}$])	λ_{em} [nm]	τ [ns]	Φ_{PL}	k_r [10^7]	k_{nr} [10^9]	$\lambda_{\text{em,FL}}$ [nm]	τ_{FL} [ns]	$\lambda_{\text{em,PH}}$ [nm]	τ_{PH} [ms]	E_T [eV]
2	258 (21900), 271 (sh), 319 (4600), 334 (4200), 368 (10600), 385 (12400), 413 (5000)	424, 446, 472, 506 (sh)	0.82	7	8.5	1.13	423, 445, 473, 505 (sh), 433, 457, 489, 530 (sh)	1.09	556, 566, 582, 603, 607, 660, 735 (sh)	63.3	2.23
<i>trans</i> - 6	270 (26500), 355 (30700), 370 (30000), 393 (sh), 414 (sh)	429, 452, 489 (sh)	0.31	6	19.3	3.03	-	0.48	-	-	-
MesDFOB	269 (32400), 330 (29100), 341 (28600), 359 (25300), 374 (sh)	366, 380	0.30	6	20.0	3.13	375, 395	0.70	436, 452, 464, 480	104	2.84

[a] Quantum yields and lifetimes determined on N_2 -saturated solutions. [FL] = fluorescence. [PH] = phosphorescence. sh = shoulder. Rate constants k_r and k_{nr} are calculated using the equations $k_r = \Phi_{\text{PL}}/\tau$ and $k_{\text{nr}} = (1-\Phi_{\text{PL}})/\tau$. Absorption and emission spectra of *trans*-**6** at r.t. are given in the SI. For absorption and emission spectra of **MesDFOB** at r.t. see reference.¹⁰

The HOMOs and LUMOs of the (BO)₂-helicenes **1** and **2** have been computed at the M06/6-311+G(d,p) level of theory (Figure 6, Figure S49). A comparison with the HOMO/LUMO of parent **7TH** confirms that the introduction of the BO moieties substantially influences the LUMO delocalization and that the Mes rings make no contribution to the frontier orbitals, in agreement with reports on (BN)-doped carbohelicenes.^{7d} The LUMO of **2** is ≈0.6 eV lower than that of **1** (–2.22 eV vs. –1.65 eV), in line with the trend observed for experimental values (–3.14 eV vs. –1.97 eV). As expected, the LUMO of **2** is mainly delocalized over the thiophene-benzene-thiophene central fragment rather than over the terminal thiophene rings (as in the case of **1**). Conversely, the HOMOs of **1**, **2**, and **7TH** present only minor differences, both in terms of energy and degree of delocalization.

Preliminary racemization tests showed that the enantiomers of **2** are stereochemically stable at room temperature. The (*P*)-/(*M*)-enantiomers of **2** were therefore separated by chiral stationary phase ultra-high performance liquid chromatography (CSP-UHPLC) on a (*S,S*)-Whelk-O 1 column, using *n*-hexane/CH₂Cl₂ (95:5) as eluent (Figure 7a).²⁴ Later, the analytical HPLC resolution was scaled up to the semipreparative level using the same eluent and a 10 mm internal diameter column. Racemization studies were conducted on the second eluted enantiomer showing an *e.e.* = 97% (*R*_t ≈ 7 min; Figure 7a, red trace). The collected fractions containing the second eluted enantiomer were combined and evaporated at room temperature. The solid residue was dissolved in decalin and subjected to thermal racemization at 80 °C.

The changes in the enantiomeric excess of the sample were checked by CSP-UHPLC (Figure 7b). The racemization process was monitored by the decrease in the enantiomeric excess of the sample. Significant interconversion of the two enantiomers was visible after 12 min and

the elution peak of the first enantiomer (*R*_t ≈ 6 min) began to emerge (Figure 7b).

After approximately 8 h, the *e.e.* had dropped to 65% (Figure 7b, purple trace). Data collected over this time (Figure S46) were used to determine the racemization constant $k_{\text{rac}} = 1.48 \times 10^{-5} \text{ s}^{-1}$.^{24,25} The enantiomerization constant was calculated by the relation $k_{\text{enant}} = 0.5 \times k_{\text{rac}}$. The free energies of activation, $\Delta G_{\text{rac}}^\ddagger = 28.6 \pm 0.1 \text{ kcal mol}^{-1}$ (at 353 K) and $\Delta G_{\text{enant}}^\ddagger = 29.4 \pm 0.1 \text{ kcal/mol}$ (at 353 K), were calculated by using the Eyring equation and setting a transmission coefficient equal to 0.5 (see Section 8.1 of the SI).²⁶ Both $\Delta G_{\text{rac}}^\ddagger$ and $\Delta G_{\text{enant}}^\ddagger$ of **2** are close to the corresponding values of **1** ($\Delta G_{\text{rac}}(\mathbf{1})^\ddagger = 26.9 \pm 0.1 \text{ kcal mol}^{-1}$, $\Delta G_{\text{enant}}(\mathbf{1})^\ddagger = 27.4 \pm 0.1 \text{ kcal mol}^{-1}$ at 353K), which reveals that the inversion of the B-O bonds does not reduce the configurational stability of the enantiomers.

We then evaluated the energy barrier through DFT calculations, using the same functional and basis set as for compound **1**.¹⁰ Optimization of the transition state has been performed at the PBE1-PBE/TZVP level with empirical dispersion corrections,²⁷ obtaining one imaginary frequency, this gave a barrier of 36 kcal mol⁻¹, significantly higher (≈ 8 kcal mol⁻¹) than the one obtained from the experimental data ($\Delta G_{\text{enant}}(\mathbf{1})^\ddagger = 27.4 \pm 0.1 \text{ kcal mol}^{-1}$). The analysis of a relaxed scan to evaluate the racemization barrier of model compounds without Mes groups (**1*** and **2***; Figure S50) allows to increase the basis set level and to compare **1*** and **2*** with **carbo[6]helicene** and **7TH** to assess the influence of the heteroatoms.²⁸ However, similar values for the enantiomerization barrier were obtained (≈ 36 kcal mol⁻¹).

By contrast, a second scan carried out for **1**, **2**, **carbo[6]helicene**, and **7TH** with a semiempirical method (AM-1 level) produced results that

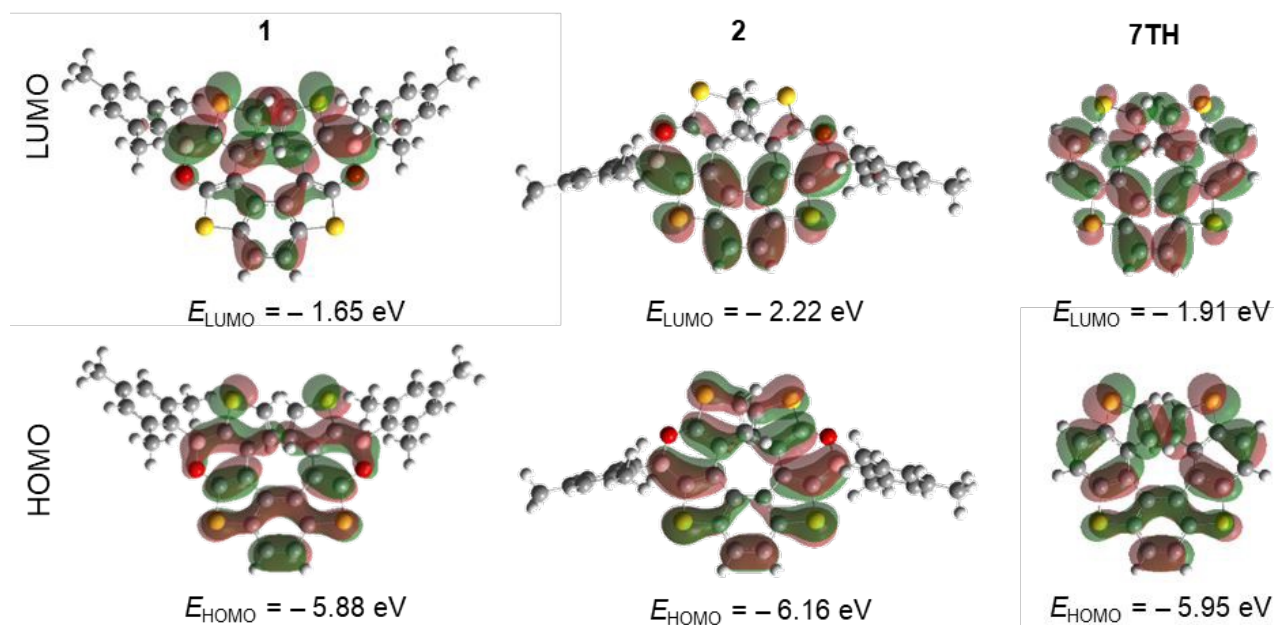


Figure 6. Isovalue surfaces for the LUMO and HOMO orbitals of **1**, **2**, and **7TH**, calculated at the M06/6-311+G(d,p) level.

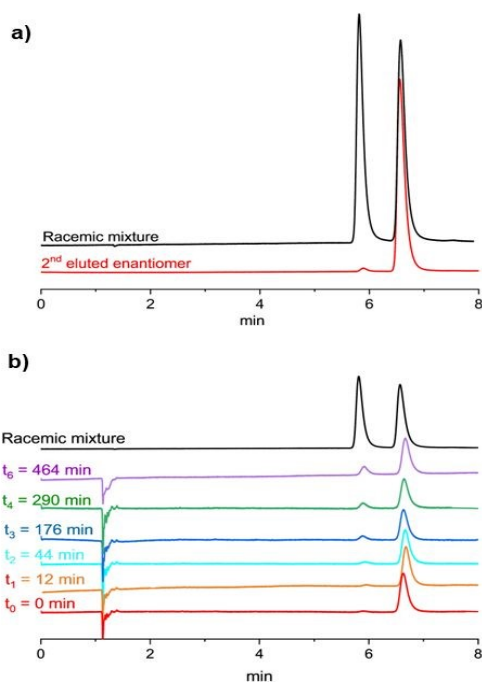


Figure 7. a) CSP-UHPLC resolution of **2** (stationary phase: (S,S)-Whelk-O 1, mobile phase: *n*-hexane/CH₂Cl₂ (95:5), flow rate = 1.0 mL min⁻¹, 25 °C). b) Thermal racemization study conducted on the second eluted enantiomer in decalin at 80 °C; solvent peak: *R*_t ≈ 1 min

were in better agreement with the experimental observations (27.8 kcal mol⁻¹ for **1** and 28.9 kcal mol⁻¹ for **2** (Figure S51). In any case, the enantiomerization barrier is not much influenced by the presence of the Mes groups. As for **1**, comparison of the minimum and transition-state structures of **2** and **7TH** suggests that the smaller double-bond character of the B=O pairs allows for greater flexibility of the six-membered heterocycles compared to benzene rings (Figure S52).¹⁰ Circular dichroism (CD) spectra recorded in *n*-hexane/CH₂Cl₂ (95:5) at 20 °C showed a perfect mirror-image relationship between the first and second eluted enantiomer of **2** (Figure 8a); the optical rotation values are -264° (*e.e.* = 98%) and +261° (*e.e.* = 97%), respectively, which are in the same order of magnitude as those of **1** (-97.5°; +97.7°).

To assign the absolute configuration, the (*M*)-structure of **2** was optimized at the M06/6-311+G(d,p) level of theory. Similar to compound **1**, only one stable conformer was found.

The comparison of calculated and experimental spectra is shown in Figure 8b: a good correspondence is obtained between the calculated spectrum and the spectrum of the first eluted enantiomer of **2** (opposite to the case of **1**, for which the (*M*)-structure matches the CD spectrum of the second eluted enantiomer). Figure 8a illustrates how the inversion of the B-O bonds leads to remarkably different CD spectra: while **1** shows only weak spectral features above λ = 260 nm,¹⁰ **2** has a more intense and structured CD spectrum with the first feature recorded at 414 nm, in correspondence of the first shoulder observed in the absorption spectrum (Figure 5a).

Circularly polarized luminescence (CPL) spectra of **2** showed a band at λ = 440 nm (Figure 8c; the resolution of our CPL apparatus does not permit to reproduce all the vibronic features observed in the

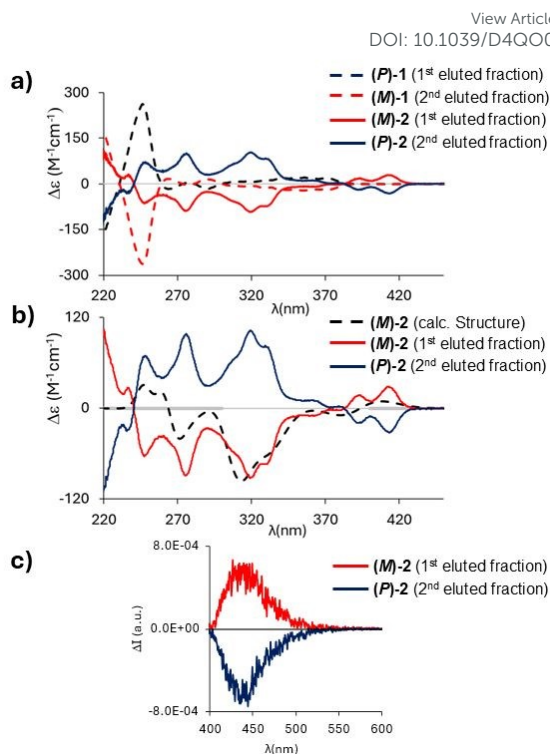


Figure 8. a) Circular dichroism (CD) spectra of the **1** (dashed lines) and **2** (solid lines) enantiomers in *n*-hexane/CH₂Cl₂ (95:5) at 20 °C; red traces correspond to the (*M*)-structures, blue traces to the (*P*)-structures. b) CD spectra of (*M*)-**2** (red trace) and (*P*)-**2** (blue trace) in *n*-hexane/CH₂Cl₂ (95:5) at 20 °C; computed CD spectrum of the optimized (*M*)-**2** structure is shown for comparison (brown dashed trace; multiplied by a factor of 1.5). c) Circularly Polarized Luminescence (CPL) spectra of (*M*)-**2** (red trace) and (*P*)-**2** (blue trace) in *n*-hexane/CH₂Cl₂ (95:5) at 20 °C.

emission spectrum of **2** (Figure 5a). The dissymmetry ratio (defined as $g_{lum} = \Delta I/I$ and $g_{abs} = \Delta A/A$)²⁹ in emission is $g_{lum} = 0.8 \times 10^{-3}$ and is comparable to those of other organic molecules,³⁰ and lower than g_{abs} of the first CD band ($g_{abs} = 2 \times 10^{-3}$; Figure 8b). The first transition, responsible for the absorption/emission band (in the two optimized geometries), is associated with an electric and magnetic dipole transition moment parallel to the C₂-axis. Interestingly, the most intense CD band ($g_{abs} = 8.5 \times 10^{-3}$) is found at 320 nm (Figure 8b); conversely, in the corresponding region of the absorption spectrum, a low-intensity band is observed (Figure 5a). This indicates that electric and magnetic dipole moments have the prevalent component along the helical axis (see Table S15).

Conclusions

We reported the synthesis and full characterization of the (BO)₂-helicene **2**, which was obtained through a four-step synthesis involving a Mallory photocyclization as last step. Moreover, the study of the synthesis of the singly-doped BO-helicene (**3**) was also described.

A combined experimental and theoretical effort allowed us to evaluate: 1) the properties-switch produced by the BO bonds inversion **1**→**2**, along with 2) the effect of BO-doping on **7TH**.

Although the effect on the quantum yield is negligible ($\Phi_{\text{PL}}(\mathbf{2}) = 7\%$ vs. $\Phi_{\text{PL}}(\mathbf{1}) = 6\%$), switching of BO vectors proved to be a useful tool to achieve a lowered LUMO, red-shifted absorption/emission bands (≈ 40 nm), and a smaller energy gap ($E_{\text{g}}^{\text{opt}}(\mathbf{2}) = 2.90$ eV vs. $E_{\text{g}}^{\text{opt}}(\mathbf{1}) = 3.16$ eV).

As previously observed for $\mathbf{1}$, comparison of $\mathbf{2}$ with $\mathbf{7TH}$, highlighted that the incorporation of BO bonds does not significantly improve fluorescence performances ($\Phi_{\text{PL}}(\mathbf{2}) = 7\%$ vs. $\Phi_{\text{PL}}(\mathbf{7TH}) = 5\%$), but provides a detectable CPL signal ($g_{\text{lum}} = 0.8 \times 10^{-3}$).

At low-temperature (77 K), $\mathbf{2}$ showed an intense and structured phosphorescence (peaked at 556 nm; $\tau = 63.3$ ms) reflecting noticeable vibronic components from "helix breathing" modes. This is important evidence that the incorporation of B-O bonds enhances the flexibility of the helical scaffold, as it is also highlighted by kinetics studies ($\Delta G_{\text{enant}}^{\ddagger}(\mathbf{2})$ is 10 kcal/mol lower than $\Delta G_{\text{enant}}^{\ddagger}(\mathbf{7TH})$).

These findings now indicate how BO-doping is a means of influencing the rigidity of tetrathia[7]helicenes and demonstrate how it is possible to manipulate the electronic distribution across the helix by changing the position of the B centers within the scaffold. Overall, our results provide essential information for the synthesis and the structural design of new (BO)-helicene derivatives with tailored optoelectronic and mechanical properties.

Author contributions

L.M. and M.W. conceived the idea. L.M., M.W., E.L., and C.B. wrote the manuscript. All authors discussed and commented on the manuscript. In detail: L.M. and C.B. synthesized the compounds; L.M. and M.P. performed spectroscopical measurements; S.A. and S.G. performed the electrochemical measurements; S.M. and C.V. performed the enantiomers separation and measured CD spectra. G.L. and G.M. performed the theoretical calculations and measured CPL spectra; A.V. and M.B. performed single crystal X-ray diffraction studies. L.M., M.W., E.L. and C.B. directed and supervised the project.

Conflicts of interest

There are no conflicts to declare.

Data availability

The data that support the findings of this study are available from the corresponding authors upon request.

Acknowledgements

L.M. is grateful to Prof. Todd B. Marder and Prof. Ivo Starý for helpful scientific discussions during the PhD defence. L. M. is grateful to the University of Milan for providing a Ph.D. scholarship and to the Goethe-Universität Frankfurt for enabling a binational joint Ph.D. programme. Parts of this research (project I-20231044) were carried out at PETRA III at DESY (Hamburg), a member of the Helmholtz Association (HGF). We thank Drs. M. Tolkiehn and E. Peresykina for their assistance regarding the use of the beamline P24 at DESY.

M.P. gratefully acknowledges Regione Lombardia and Fondazione Cariplo for funding the SmartMatLab Center project.

Notes and references

View Article Online

DOI: 10.1039/D4QO01897D

1 a) J. Crassous, I. G. Stará and I. Starý, *Helicenes: Synthesis, Properties and Applications*, John Wiley & Sons, 2022; b) C.-F. Chen and Y. Shen, *Helicene Chemistry*, Springer, 2017; c) P. Ravat, Carbo[n]helicenes Restricted to Enantiomerize: An Insight into the Design Process of Configurationally Stable Functional Chiral PAHs, *Chem. - A Eur. J.*, 2021, **27**, 3957–3967; d) G. Gingras, One hundred years of helicene chemistry. Part 3: applications and properties of carbohelicenes, *Chem. Soc. Rev.*, 2013, **42**, 1051–1095; e) J. M. Fernández-García, P. J. Evans, S. Filippone, M. Á. Herranz and N. Martín, Chiral Molecular Carbon Nanostructures, *Acc. Chem. Res.*, 2019, **52**, 1565–1574.

2 a) S. Abbate, G. Longhi and T. Mori, *Helicenes: Chiroptical Properties of Helicenes*, John Wiley & Sons, 2022, 373–394; b) T. Mori, Chiroptical Properties of Symmetric Double, Triple, and Multiple Helicenes, *Chem. Rev.*, 2021, **121**, 2373–2412; c) P. Izquierdo-García, J. M. Fernández-García, S. Medina Rivero, M. Šámal, J. Rybáček, L. Bednárová, S. Ramírez-Barroso, F. J. Ramírez, R. Rodríguez, J. Perles, D. García-Fresnadillo, J. Crassous, J. Casado, I. G. Stará and N. Martín, Helical Bilayer Nanographenes: Impact of the Helicene Length on the Structural, Electrochemical, Photophysical, and Chiroptical Properties, *J. Am. Chem. Soc.*, 2023, **145**, 11599–11610.

3 a) S. T. J. Ryan and M. J. Fuchter, *Helicenes: Helicenes for Optoelectronic Applications and Devices*, John Wiley & Sons, 2022, 473–503; b) J. R. Brandt, F. Salerno and M. J. Fuchter, The added value of small-molecule chirality in technological applications, *Nat. Rev. Chem.*, 2017, **1**, 17–45; c) H. Isla and J. Crassous, Helicene-based chiroptical switches, *Comptes Rendus Chim.*, 2016, **19**, 39–49. d) K. Dhbaibi, L. Abella, S. Meunier-Della-Gatta, T. Roisnel, N. Vanthuynne, B. Jamoussi, G. Pieters, B. Racine, E. Quesnel, J. Autschbach, J. Crassous and L. Favereau, Achieving high circularly polarized luminescence with push-pull helicenic systems: from rationalized design to top-emission CP-OLED applications, *Chem. Sci.*, 2021, **12**, 5522–5533.

4 a) A. Borissov, Y. K. Maurya, L. Moshniha, W. S. Wong, M. Żyła-Karwowska and M. Stępień, Recent Advances in Heterocyclic Nanographenes and Other Polycyclic Heteroaromatic Compounds, *Chem. Rev.*, 2022, **122**, 565–788; b) M. Hirai, N. Tanaka, M. Sakai and S. Yamaguchi, Structurally Constrained Boron-, Nitrogen-, Silicon-, and Phosphorus-Centered Polycyclic π -Conjugated Systems, *Chem. Rev.*, 2019, **119**, 8291–8331; c) E. von Grotthuss, A. John, T. Kaese and M. Wagner, Doping Polycyclic Aromatics with Boron for Superior Performance in Materials Science and Catalysis, *Asian J. Org. Chem.*, 2018, **7**, 37–53; d) M. Stępień, E. Gońka, M. Żyła and N. Sprutta, Heterocyclic Nanographenes and Other Polycyclic Heteroaromatic Compounds: Synthetic Routes, Properties, and Applications, *Chem. Rev.*, 2017, **117**, 3479–3716.

5 a) A. Nowak-Król, P. T. Geppert and K. R. Naveen, Boron-containing helicenes as new generation of chiral materials:

 Downloaded on 12/20/24 7:55:10 AM
 This article is licensed under a Creative Commons Attribution-NonCommercial 3.0 Unported Licence.


opportunities and challenges of leaving the flatland, *Chem. Sci.*, 2024, **15**, 7408–7440; b) K. Dhbaibi, L. Favereau and J. Crassous, Enantioenriched Helicenes and Helicenoids Containing Main-Group Elements (B, Si, N, P), *Chem. Rev.*, 2019, **119**, 8846–8953.

6 For related B(sp²)-doped helicenes/helicely-chiral PAHs, see: a) M. Schnitzlein, K. Shoyama and F. Würthner, A highly fluorescent bora[6]helicene exhibiting circularly polarized light emission, *Chem. Sci.*, 2024, **15**, 2984–2989; b) W. Sun, J. Guo, Z. Fan, L. Yuan, K. Ye, C. Dou and Y. Wang, Ribbon-Type Boron-Doped Polycyclic Aromatic Hydrocarbons: Conformations, Dynamic Complexation and Electronic Properties, *Angew. Chemie - Int. Ed.*, 2022, **61**, e202209271; c) F. Miyamoto, S. Nakatsuka, K. Yamada, K. I. Nakayama and T. Hatakeyama, Synthesis of Boron-Doped Polycyclic Aromatic Hydrocarbons by Tandem Intramolecular Electrophilic Arene Borylation, *Org. Lett.*, 2015, **17**, 6158–6161; d) J. Radtke, K. Schickedanz, M. Bamberg, L. Menduti, D. Schollmeyer, M. Bolte, H. W. Lerner and M. Wagner, Selective access to either a doubly boron-doped tetrabenzopentacene or an oxadiborepin from the same precursor, *Chem. Sci.*, 2019, **10**, 9017–9027; e) K. Schickedanz, T. Trageser, M. Bolte, H. W. Lerner and M. Wagner, A boron-doped helicene as a highly soluble, benchtop-stable green emitter, *Chem. Commun.*, 2015, **51**, 15808–15810. f) Y. Liu, L. Yuan, Z. Fan, J. Yang, Y. Wang and C. Dou, Boron-doped double [6]carbohelicenes: a combination of helicene and boron-doped π -systems, *Chem. Sci.*, 2024, **15**, 12819–12826; g) A. Ikeno, M. Hayakawa, M. Sakai, Y. Tsutsui, S. Nakatsuka, S. Seki and T. Hatakeyama, π -Extended 9b-Boraphenalenenes: Synthesis, Structure, and Physical Properties, *J. Am. Chem. Soc.*, 2024, **146**, 17084–17093.

7 For related B(sp²)-N doped helicenes/ helicely-chiral PAHs, see: a) Y. Appiaris, S. Míguez-Lago, P. Puylaert, N. Wolf, S. Kumar, M. Molkenhain, D. Miguel, T. Neudecker, M. Juríček, A. G. Campaña and A. Staubitz, Boosting quantum yields and circularly polarized luminescence of penta- and hexahelicenes by doping with two BN-groups, *Chem. Sci.*, 2024, **5**, 466–476; b) A. Abengózar, P. García-García, D. Sucunza, A. Pérez-Redondo and J. J. Vaquero, Synthesis of functionalized helical BN-benzo[c]phenanthrenes, *Chem. Commun.*, 2018, **54**, 2467–2470; c) Z. Sun, C. Yi, Q. Liang, C. Bingi, W. Zhu, P. Qiang, D. Wu and F. Zhang, π -Extended C₂-Symmetric Double NBN-Heterohelicenes with Exceptional Luminescent Properties, *Org. Lett.*, 2020, **22**, 209–213; d) F. Zhang, F. Rauch, A. Swain, T. B. Marder and P. Ravat, Efficient Narrowband Circularly Polarized Light Emitters Based on 1,4-B,N-embedded Rigid Donor-Acceptor Helicenes, *Angew. Chemie - Int. Ed.*, 2023, **62**, 1–7; e) K. Yuan, D. Volland, S. Kirschner, M. Uzelac, G. S. Nichol, A. Nowak-Król and M. J. Ingleson, Enhanced N-directed electrophilic C–H borylation generates BN-[5]- and [6]helicenes with improved photophysical properties, *Chem. Sci.*, 2022, **13**, 1136–1145; f) M. Yang, I. S. Park and T. Yasuda, Full-Color, Narrowband, and High-Efficiency Electroluminescence from Boron and Carbazole Embedded Polycyclic Heteroaromatics, *J. Am. Chem. Soc.*, 2020, **142**, 19468–19472; g) J. K. Li, X. Y. Chen, Y. L. Guo, X. C. X. Y. Wang, A. C. H. Sue, X. Y. Cao and X. C. X. Y. Wang, B, N-embedded double hetero[7]helicenes with strong chiroptical responses in the


visible light region, *J. Am. Chem. Soc.*, 2021, **143**, 17958–17963. h) T. Hatakeyama, S. Hashimoto, T. Oba and M. Nakamura, Azaboradibenzo[6]helicene: carrier inversion induced by helical homochirality, *J. Am. Chem. Soc.*, 2012, **134**, 19600–19603; i) Y. Si and G. Yang, Photophysical properties of azaboradibenzo[6]helicene derivatives, *J. Mater. Chem. C*, 2013, **1**, 2354–2361; j) G. Meng, J. Zhou, X. S. Han, W. Zhao, Y. Zhang, M. Li, C. F. Chen, D. Zhang and L. Duan, B-N Covalent Bond Embedded Double Hetero-[n]helicenes for Pure Red Narrowband Circularly Polarized Electroluminescence with High Efficiency and Stability, *Adv. Mater.*, 2024, **36**, 1–11; k) Y. Jiao, Z. Sun, Z. Wang, Y. Fu and F. Zhang, Synthesis of Nonsymmetric NBN-Embedded [6]- and [7]Helicenes with Amplified Activities, *Org. Lett.*, 2023, **25**, 8766–8770; l) D. Tan, J. Dong, T. Ma, Q. Feng, S. Wang and D. T. Yang, Multiple helicenes defected by heteroatoms and heptagons with narrow emissions and superior photoluminescence quantum yields, *Angew. Chemie - Int. Ed.*, 2023, **62**, e202304711.

8 For related B(sp²)-O doped helicenes/ helicely-chiral PAHs, see: a) T. Katayama, S. Nakatsuka, H. Hirai, N. Yasuda, J. Kumar, T. Kawai and T. Hatakeyama, Two-step synthesis of boron-fused double helicenes, *J. Am. Chem. Soc.*, 2016, **138**, 5210–5213; b) X. Y. Wang, A. Narita, W. Zhang, X. Feng and K. Müllen, Synthesis of stable nanographenes with OBO-doped zigzag edges based on tandem demethylation-electrophilic borylation, *J. Am. Chem. Soc.*, 2016, **138**, 9021–9024; c) X. Y. Wang, T. Dienel, M. Di Giovannantonio, G. B. Barin, N. Kharche, O. Deniz, J. I. Urgel, R. Widmer, S. Stolz, L. H. De Lima, M. Muntwiler, M. Tommasini, V. Meunier, P. Ruffieux, X. Feng, R. Fasel, K. Müllen and A. Narita, Heteroatom-doped perihexacene from a double helicene precursor: on-surface synthesis and properties, *J. Am. Chem. Soc.*, 2017, **139**, 4671–4674; d) Z. Zhou, X. Y. Wang, Z. Wei, K. Müllen and M. A. Petrukhina, Charging OBO-Fused Double[5]Helicene with Electrons, *Angew. Chemie - Int. Ed.*, 2019, **58**, 14969–14973.

9 For related B(sp³)-N doped helicenes/helicely-chiral PAHs, see: a) F. Full, A. Artigas, K. Wiegand, D. Volland, K. Szkodzińska, Y. Coquerel and A. Nowak-Król, Controllable 1,4-Palladium Aryl to Aryl Migration in Fused Systems – Application to the Synthesis of Azaborole Multihelicenes, *J. Am. Chem. Soc.*, 2024, **146**, 29245–29254; b) D. Volland, J. Niedens, P. T. Geppert, M. J. Wildervanck, F. Full and A. Nowak-Król, Synthesis of a Blue-Emissive Azaborathia[9]helicene by Silicon-Boron Exchange from Unusual Atropisomeric Teraryls, *Angew. Chemie - Int. Ed.*, 2023, **62**, e202304291; c) F. Full, M. J. Wildervanck, D. Volland and A. Nowak-Król, Synthesis of Enantioenriched Azaborole Helicenes by Chirality Transfer from Axially Chiral Biaryls, *Synlett*, 2023, **34**, 477–482; d) J. Full, S. P. Panchal, J. Götz, A. M. Krause and A. Nowak-Król, Modular synthesis of organoboron helically chiral compounds: cutouts from extended helices, *Angew. Chemie - Int. Ed.*, 2021, **60**, 4350–4357; e) Z. Domínguez, R. López-Rodríguez, E. Álvarez, S. Abbate, G. Longhi, U. Pischel and A. Ros, Azabora[5]helicene Charge-Transfer Dyes Show Efficient and Spectrally Variable Circularly Polarized Luminescence, *Chem. - A Eur. J.*, 2018, **24**, 12660–12668; f) C. Shen, M. Srebro-Hooper, M. Jean, N. Vanthuyne, L. Toupet, J. A. G.

- Williams, A. R. Torres, A. J. Riives, G. Muller, J. Autschbach and J. Crassous, Synthesis and chiroptical properties of hexa-, octa-, and deca-azaborahelicenes: influence of helicene size and of the number of boron atoms, *Chem. - A Eur. J.*, 2017, **23**, 407–418.
- 10 L. Menduti, C. Baldoli, S. Manetto, M. Bolte, H. W. Lerner, G. Longhi, C. Villani, E. Licandro and M. Wagner, (BO)₂-Doped Tetrathia[7]helicene: A Configurationally Stable Blue Emitter, *Angew. Chemie - Int. Ed.*, 2023, **62**, e202215468.
- 11 A. Bossi, P. R. Mussini, G. Farinola, M. Penconi, S. Cauteruccio, M. E. Thompson and E. Licandro, Sparkling Organic Phosphorescence from Fluorinated Tetrathia[7]helicenes: Synthesis and Photophysical, Electrochemical and Computational Studies, *Chem. - A Eur. J.*, 2023, **29**, e202300339.
- 12 Commercially available compound: CAS 18791-75-8.
- 13 S. A. Iqbal, J. Pahl, K. Yuan and M. J. Ingleson, Intramolecular (directed) electrophilic C–H borylation, *Chem. Soc. Rev.*, 2020, **49**, 4564–4591.
- 14 K. B. Jørgensen, Photochemical oxidative cyclisation of stilbenes and stilbenoids - the Mallory-reaction, *Molecules*, 2010, **15**, 4334–4358.
- 15 H. Nakagawa, A. Obata, K. I. Yamada, H. Kawazura, M. Konno and H. Miyamae, Crystal and Molecular Structures of Tetrathia[7]heterohelicene: Racemate and Enantiomer, *J. Chem. Soc. Perkin Trans. II*, 1985, **20**, 1899–1903.
- 16 C. Hoffend, M. Diefenbach, E. Januszewski, M. Bolte, H. W. Lerner, M. C. Holthausen and M. Wagner, Effects of boron doping on the structural and optoelectronic properties of 9,10-diarylanthracenes, *Dalt. Trans.*, 2013, **42**, 13826–13837.
- 17 A. Budanow, E. Von Grothuss, M. Bolte, M. Wagner and H. Lerner, 10,9-Oxaboraphenanthrenes as luminescent fluorophores, *Tetrahedron*, 2016, **72**, 1477–1484.
- 18 Deposition numbers CCDC 2384683 (for **2**), CCDC 2384684 (for **4**), CCDC 2384685 (for **5**), CCDC 2384686 (for **6**), CCDC 2384687 (for **7**), CCDC 2384688 (for **8**), CCDC 2384689 (for **9**), CCDC 2384690 (for **10**) and CCDC 2384691 (for **11**) contain the supplementary crystallographic data for this paper. These data are provided free of charge by the joint Cambridge Crystallographic Data Centre and Fachinformati-onszentrum Karlsruhe Access Structures service.
- 19 Propylene oxide is a known scavenger for the HI developed during photocyclizations carried out using I₂ as oxidant: L. Liu, B. Yang, T. J. Katz and M. K. Poindexter, Improved methodology for photocyclization reactions, *J. Org. Chem.*, 1991, **56**, 3769–3775.
- 20 T. Caronna, M. Catellani, S. Luzzati, L. Malpezzi, S. V. Meille, A. Mele, C. Richter and R. Sinisi, Molecular crystal architecture and optical properties of a thiohelicenes series containing 5, 7, 9, and 11 rings prepared via photochemical synthesis, *Chem. Mater.*, 2001, **13**, 3906–3914. DOI: 10.1039/D4QO01897D
- 21 a) C. Johannessen, E. W. Blanch, C. Villani, S. Abbate, G. Longhi, N. R. Agarwal, M. Tommasini and D. A. Lightner, Raman and ROA spectra of (–)- and (+)-2-Br-Hexahelicene: Experimental and DFT Studies of a π-Conjugated Chiral System, *J. Phys. Chem. B*, 2013, **117**, 2221–2230; b) F. Della Sala, V. Vitale, M. Mazzeo, R. Cingolani, G. Gigli, L. Favaretto and G. Barbarella, The effects of oxygen and boron functionalization on the optical properties of dithienothiophenes, *J. Non. Cryst. Solids*, 2006, **352**, 2461–2464; c) Z. Sun, W. Xu, S. Qiu, Z. Ma, C. Li, S. Zhang and H. Wang, Thia[n]helicenes with long persistent phosphorescence, *Chem. Sci.*, 2024, **15**, 1077–1087; d) Y. Kondo, Y. Tsutsui, Y. Matsuo, T. Tanaka and S. Seki, Impacts of heteroatom substitution on the excited state dynamics of π-extended helicenes, *Nanoscale Adv.*, 2024, **6**, 4567–4571.
- 22 S. P. McGlynn and T. Azumi, Molecular spectroscopy of the triplet state, *Prentice-Hall*, 1969.
- 23 L. Menduti, C. Baldoli, S. Arnaboldi, A. Dreuw, D. Tahaoglu, A. Bossi and E. Licandro, (Dimesityl)boron Benzodithiophenes: Synthesis, Electrochemical, Photophysical and Theoretical Characterization, *ChemistryOpen*, 2022, **11**, 1–11.
- 24 Full details are given in the Supporting Information.
- 25 a) L. Meca, D. Reha and Z. Havlas, Racemization Barriers of 1,1'-Binaphthyl and 1,1'-Binaphthalene-2,2'-diol: A DFT Study, *J. Org. Chem.*, 2003, **68**, 5677–5680; b) D. C. Patel, R. M. Woods, Z. S. Breitbach, A. Berthod and D. W. Armstrong, Thermal racemization of biaryl atropisomers, *Tetrahedron Asymmetry*, 2017, **28**, 1557–1561.
- 26 Enantiomerization is the reversible conversion of a single enantiomer into the other one. The corresponding rate constant is k_{enant} . Racemization is the irreversible conversion of a sample of single enantiomers or of a non-racemic mixture of enantiomers into the racemate. The corresponding rate constant is k_{rac} . Comparison of calculated and experimental energy barriers was done using the enantiomerization barrier obtained from k_{enant} , which is calculated from the experimentally determined k_{rac} according to: $k_{\text{enant}} = 0.5k_{\text{rac}} = 8.15 \times 10^{-5} \text{ s}^{-1}$. The free energy for the enantiomerization process ($\Delta G_{\text{enant}}^\ddagger$) was obtained by using the Eyring equation and setting a transmission equal to 0.5.
- 27 a) S. Grimme, J. Antony, S. Ehrlich and H. Krieg, A consistent and accurate ab initio parametrization of density functional dispersion correction (DFT-D) for the 94 elements H-Pu, *J. Chem. Phys.*, 2010, **132**, 154104; b) J. Barroso, J. L. Cabellos, S. Pan, F. Murillo, X. Zarate, M. A. Fernandez-Herrera and G. Merino, Revisiting the racemization mechanism of helicenes, *Chem. Commun.*, 2017, **54**, 188–191.
- 28 a) For experimental data on **7TH** racemization see: K. Yamada, H. Nakagawa and H. Kawazura, Thermal racemization of thiaheterohelicenes, *Bull. Chem. Soc. Jpn.*, 1986, **59**, 2429–2432; b) for experimental data on **carbo[6]helicene** racemization see: R. H.

Downloaded on 20/04/2024 7:35:10 AM
 This article is published under a Creative Commons Attribution-NonCommercial 3.0 Unported Licence.



Journal Name

ARTICLE

Janke, G. Haufe, E. U. Würthwein and J. H. Borkent, Racemization Barriers of Helicenes: A Computational Study, *J. Am. Chem. Soc.*, 1996, **118**, 6031–6035.

View Article Online
DOI: 10.1039/D4QO01897D

29 a) W. Kuhn, The physical significance of optical rotatory power, *Z. Physik. Chem.* 1929, **B4**, 14–36; b) W. Kuhn, Optical rotatory power, *Annu. Rev. Phys. Chem.* 1958, **9**, 417–438.

30 a) Y. Liu, J. Cerezo, G. Mazzeo, N. Lin, X. Zhao, G. Longhi, S. Abbate and F. Santoro, Vibronic coupling explains the different shape of electronic circular dichroism and of circularly polarized luminescence spectra of hexahelicenes, *J. Chem. Theory Comput.*, 2016, **12**, 2799–2819; b) H. Tanaka, Y. Inoue and T. Mori, Circularly polarized luminescence and circular dichroisms in small organic molecules: correlation between excitation and emission dissymmetry factors, *ChemPhotoChem*, 2018, **2**, 386–402.

1
2
3 **(BO)₂-doped tetrathia[7]helicenes: synthesis and properties-change induced by “BO bonds inversion”** View Article Online
4 Luigi Menduti,* Clara Baldoli, Simone Manetto, Claudio Villani, Marta Penconi, Sara Grecchi, Serena Arnaboldi, Giuseppe Mazzeo, Giovanna
5 Longhi, Michael Bolte, Alexander Virovets, Hans-Wolfram Lerner, Matthias Wagner* and Emanuela Licandro
6

7 The data supporting this article have been included as part of the Supplementary Information.

8
9 The CIF files containing the crystallographic information are deposited in the Cambridge Crystallographic Data Centre under
10 the deposition codes **2384683-2384691** and can be obtained free of charge via www.ccdc.cam.ac.uk/data_request/cif.
11 Deposition numbers CCDC **2384683** (for 2), CCDC **2384684** (for 4), CCDC **2384685** (for 5), CCDC **2384686** (for 6), CCDC
12 **2384687** (for 7), CCDC **2384688** (for 8), CCDC **2384689** (for 9), CCDC **2384690** (for 10) and CCDC **2384691** (for 11) contain
13 the supplementary crystallographic data for this paper.
14

15
16
17 Luigi Menduti



18
19
20
21
22
23
24
25
26
27
28
29
30
31
32
33
34
35
36
37
38
39
40
41
42
43
44
45
46
47
48
49
50
51
52
53
54
55
56
57
58
59
60
61
62
63
64
65
66
67
68
69
70
71
72
73
74
75
76
77
78
79
80
81
82
83
84
85
86
87
88
89
90
91
92
93
94
95
96
97
98
99
100
101
102
103
104
105
106
107
108
109
110
111
112
113
114
115
116
117
118
119
120
121
122
123
124
125
126
127
128
129
130
131
132
133
134
135
136
137
138
139
140
141
142
143
144
145
146
147
148
149
150
151
152
153
154
155
156
157
158
159
160
161
162
163
164
165
166
167
168
169
170
171
172
173
174
175
176
177
178
179
180
181
182
183
184
185
186
187
188
189
190
191
192
193
194
195
196
197
198
199
200
201
202
203
204
205
206
207
208
209
210
211
212
213
214
215
216
217
218
219
220
221
222
223
224
225
226
227
228
229
230
231
232
233
234
235
236
237
238
239
240
241
242
243
244
245
246
247
248
249
250
251
252
253
254
255
256
257
258
259
260
261
262
263
264
265
266
267
268
269
270
271
272
273
274
275
276
277
278
279
280
281
282
283
284
285
286
287
288
289
290
291
292
293
294
295
296
297
298
299
300
301
302
303
304
305
306
307
308
309
310
311
312
313
314
315
316
317
318
319
320
321
322
323
324
325
326
327
328
329
330
331
332
333
334
335
336
337
338
339
340
341
342
343
344
345
346
347
348
349
350
351
352
353
354
355
356
357
358
359
360
361
362
363
364
365
366
367
368
369
370
371
372
373
374
375
376
377
378
379
380
381
382
383
384
385
386
387
388
389
390
391
392
393
394
395
396
397
398
399
400
401
402
403
404
405
406
407
408
409
410
411
412
413
414
415
416
417
418
419
420
421
422
423
424
425
426
427
428
429
430
431
432
433
434
435
436
437
438
439
440
441
442
443
444
445
446
447
448
449
450
451
452
453
454
455
456
457
458
459
460
461
462
463
464
465
466
467
468
469
470
471
472
473
474
475
476
477
478
479
480
481
482
483
484
485
486
487
488
489
490
491
492
493
494
495
496
497
498
499
500
501
502
503
504
505
506
507
508
509
510
511
512
513
514
515
516
517
518
519
520
521
522
523
524
525
526
527
528
529
530
531
532
533
534
535
536
537
538
539
540
541
542
543
544
545
546
547
548
549
550
551
552
553
554
555
556
557
558
559
560
561
562
563
564
565
566
567
568
569
570
571
572
573
574
575
576
577
578
579
580
581
582
583
584
585
586
587
588
589
590
591
592
593
594
595
596
597
598
599
600
601
602
603
604
605
606
607
608
609
610
611
612
613
614
615
616
617
618
619
620
621
622
623
624
625
626
627
628
629
630
631
632
633
634
635
636
637
638
639
640
641
642
643
644
645
646
647
648
649
650
651
652
653
654
655
656
657
658
659
660
661
662
663
664
665
666
667
668
669
670
671
672
673
674
675
676
677
678
679
680
681
682
683
684
685
686
687
688
689
690
691
692
693
694
695
696
697
698
699
700
701
702
703
704
705
706
707
708
709
710
711
712
713
714
715
716
717
718
719
720
721
722
723
724
725
726
727
728
729
730
731
732
733
734
735
736
737
738
739
740
741
742
743
744
745
746
747
748
749
750
751
752
753
754
755
756
757
758
759
760
761
762
763
764
765
766
767
768
769
770
771
772
773
774
775
776
777
778
779
780
781
782
783
784
785
786
787
788
789
790
791
792
793
794
795
796
797
798
799
800
801
802
803
804
805
806
807
808
809
810
811
812
813
814
815
816
817
818
819
820
821
822
823
824
825
826
827
828
829
830
831
832
833
834
835
836
837
838
839
840
841
842
843
844
845
846
847
848
849
850
851
852
853
854
855
856
857
858
859
860
861
862
863
864
865
866
867
868
869
870
871
872
873
874
875
876
877
878
879
880
881
882
883
884
885
886
887
888
889
890
891
892
893
894
895
896
897
898
899
900
901
902
903
904
905
906
907
908
909
910
911
912
913
914
915
916
917
918
919
920
921
922
923
924
925
926
927
928
929
930
931
932
933
934
935
936
937
938
939
940
941
942
943
944
945
946
947
948
949
950
951
952
953
954
955
956
957
958
959
960
961
962
963
964
965
966
967
968
969
970
971
972
973
974
975
976
977
978
979
980
981
982
983
984
985
986
987
988
989
990
991
992
993
994
995
996
997
998
999
1000

Milan, October 8th, 2024

